Defocus electron microscopy of multiphase polymers: use and misuse

Eric J. Roche* **and Edwin L. Thomas**
Polymer Science and Engineering Department, The University of Massachusetts, Amherst, Massachusetts 01003, *USA*
(*Received* 18 *February* 1980; *revised* 22 *April* 1980)

Application of defocus microscopy to the imaging of multiphase polymers is investigated. Theoretical image contrast of ideally phase separated, model objects is predicted by application of the transfer theory of imaging. The calculations are in good agreement with observed images of a polypropylene film. Easy recognition of the cross-hatched structure of polypropylene, however, necessitates the use of very high defocus values. Application of this defocus technique to more complex systems causes problems. Defocused images of a polyurethane film are found to be indistinguishable from those of a carbon film or an amorphous polystyrene film, i.e. the image is dominated by the spatially filtered noise structure. It is suggested that previous electron micrographs of domain structures of polyurethanes have been misinterpreted.

INTRODUCTION

A significant problem in studies of polymer morphology by electron microscopy is obtaining sufficient contrast in electron micrographs to visualize the structures. Since even in well phase separated systems (i.e., pure component phases with sharp phase boundaries) the regions are of similar electron density, mass thickness contrast is intrinsically low. When diffraction contrast can be used, or if a specific heavy atom stain is available, unambiguous interpretation is generally possible. If these techniques cannot be employed, phase contrast is the only source of contrast available.

Phase contrast is intrinsic to the electron microscope due to the high coherence of the electron beam and has long been known as a way of enhancing image contrast[1]. Its application to biological specimens has been investigated in detail[2]. In the polymer field, images from a variety of homopolymer amorphous films initially interpreted as indicating an ordered nodular structure[3-9], as opposed to the random coil model[10], are in fact explained by phase contrast effects[11]. Another controversial case is that of segmented copolymers. For example, some authors have interpreted the small scale structure observed in electron micrographs of polyurethanes as corresponding to segmented hard and soft domains[12-14]. More recently, Peterman and Miles have proposed phase (defocus) contrast as a routine technique to study polymer microstructure[15].

At the same time, however, a number of papers have warned about the dangers of any naive interpretation of phase contrast structures. Some typical cases of misinterpretation of the fine structure of cellulose and keratin fibres were reviewed by Johnson and Crawford in 1973[16]. Other examples are cited in reference 17. Unfortunately, it seems that polymer morphologists have not benefitted from these works as many of the subsequently published electron micrographs of polymer 'microdomains' have been interpreted without consideration of the transfer properties of the electron microscope. In this paper the use of defocus contrast to study multiphase polymer microstructure is investigated. Theoretically predicted images of model structures are compared with experimental images of several different polymer films.

* On leave from the CERMAV-CNRS, Grenoble, France

THEORETICAL BACKGROUND

Transfer theory

The effect of microscope defocus on the images of thin films is best understood in terms of the transfer theory of imaging. Detailed explanations of this theory have been given in many articles[18-20]. A simplified presentation for its application to polymers has been presented in a previous paper[11], where the emphasis was on dark field imaging. This theory is applicable to the case of pure polymer specimens. Built of light atoms, these specimens do not significantly alter the amplitude of the electron waves so that the object function consists only of a phase term, $\exp[i\psi(\mathbf{r})]$. Further, this modulation is small compared to unity (the so-called weak phase object), which allows the approximation

$$\exp i\psi(\mathbf{r}) \simeq 1 + i\psi(\mathbf{r}) \tag{1}$$

Under these conditions, the electron microscope works as a linear imaging system so that a simple linear relation exists (for axial bright field) between the Fourier transform of the image intensity $\mathbf{I}(\mathbf{r})$ and the Fourier transform ($\mathscr{F}$) of the object function ($\psi(\mathbf{r})$):

$$\mathscr{F}\{\mathbf{I}(\mathbf{r})\} = \delta(\mathbf{K}) - 2T(\mathbf{K})\,\mathscr{F}\{\psi(\mathbf{r})\} \tag{2}$$

The electron microscope transfer function $T(\mathbf{K})$ has the form:

$$T(\mathbf{K}) = A(\mathbf{K}) \sin \chi(\mathbf{K}) \tag{3}$$

0032-3861/81/030333-09$02.00

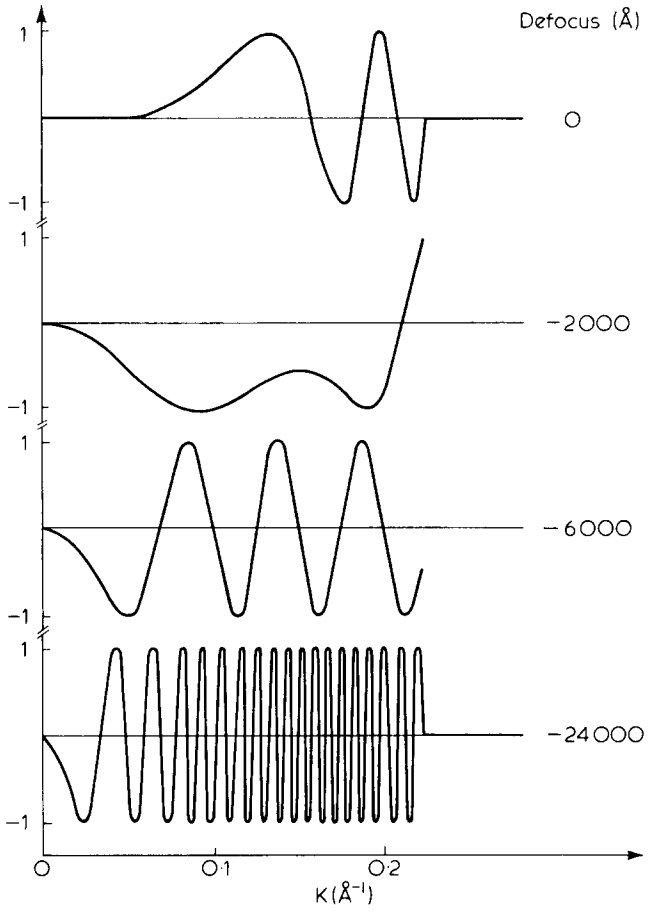

Figure 1 Variation of the transfer function, sin χ, with defocus; C_S = 6.7 mm

with imaging system phase shift $\chi(\mathbf{K})$ given by:

$$\chi(\mathbf{K}) = \pi\lambda(\Delta z)K^2 + \frac{\pi}{2}C_s\lambda^3K^4 \qquad (4)$$

and $A(\mathbf{K}) = 1/0$ inside/outside the objective aperture. Δz and C_s are the defocus and spherical aberration of the objective lens and K is the modulus of the reciprocal space difference scattering vector between the incident wave vector $\mathbf{k}$ and scattered wave vector $\mathbf{k}'$. This formulation neglects higher order terms due to chromatic aberration and beam divergence effects — approximations justified by the medium resolution conditions generally selected for polymer specimens.

In certain cases (thicker and/or higher atomic number specimens) amplitude contrast must be taken into account. A simple way to account for a small amplitude contribution is to add a constant term K_0 to the reciprocal space variable K in equation (2)[19]. If, instead the image intensity, $i(r)$ is defined as the image contrast $\frac{I - I_{av}}{I_{av}}$, equation (2) becomes:

$$\mathcal{F}\{I(\mathbf{r})\} = -2A(\mathbf{K}) \sin \chi(\mathbf{K}) \; \mathcal{F}\{\psi(\mathbf{r})\} \qquad (5)$$

It must be noted that $\mathbf{r}$ and $\mathbf{K}$ are two dimensional vectors. To avoid lengthy calculations, the one dimensional version of equation (5) is effectively taken as an approximation. The one dimensional treatment is, however, rigorous only for objects consisting of elongated parallel domains (*Figure* 2*a*) as will be considered below.

Application of a reciprocal Fourier transfrom to equation (5) gives:

$$I(r) = \mathcal{F}^{-1}\{-2A(K)\sin \chi(K)\mathcal{F}[\psi(r)]\} \qquad (6)$$

This equation is the basis for model calculations. The effect of the transfer function is to modulate particular object frequencies in the image. Sin χ can be adjusted by means of objective lens defocus (sin χ is a sensitive function of defocus, see *Figure* 1) in order to highlight selected frequencies corresponding to object details of interest. This is the fundamental principle of phase (defocus) contrast microscopy.

The object function

The object function $\psi(r)$ is the phase shift of the incident electron wave passing through the object and is directly proportional to the mean inner potential $[\bar{\varphi}(r)]$ of the specimen:

$$\psi(\mathbf{r}) = \frac{\pi}{\lambda V_0} t\bar{\varphi}(\mathbf{r}) \qquad (7)$$

where λ is the wavelength of the electron, V_0 the accelerating voltage and t the specimen thickness.

In the case of crystalline solids, the mean inner potential (in volts) may be approximated by[21]:

$$\bar{\varphi} = 114.5\frac{\sum_i f_i}{\Omega} \qquad (8)$$

where f_i is the electron scattering factor (in dimensionless p-units) at zero angle of the ith atom in the unit cell of volume Ω (in Å^3). Equation (8) can be extended to noncrystalline solids by selecting Ω as the elementary volume occupied by the structural molecular unit. Introducing the density ρ(g cm^{-3}) of the material and the molecular weight, M (g), of the structural unit, we have:

$$\bar{\varphi} = 69\frac{\rho}{M}\sum_i f_i \qquad (9)$$

which, with the aid of equation (7), allows calculation of the projected phase shift at any point of the exit face of the object. We must note, however, that the value of practical interest is not $\psi(\mathbf{r})$ but $\Delta\psi(\mathbf{r})$, the relative projected phase change, obtained after subtraction of the average background phase change.

PRACTICAL CONSIDERATIONS: APPLICATION TO TYPICAL POLYMER FILMS

Geometrical factors

Before making any calculations, possible film geometries must be considered. The variation of the projected phase change is due to the difference in mean inner potential between phases and, moreover, the shape and distribution of the polymer phases throughout the specimen thickness. *Figure* 2 illustrates two possible geometries, in the case where two phases are present. In *Figure* 2*b* the domains are small compared to the film thickness and packed at random. Whatever the intrinsic relative phase change between the two polymer phases, the resulting

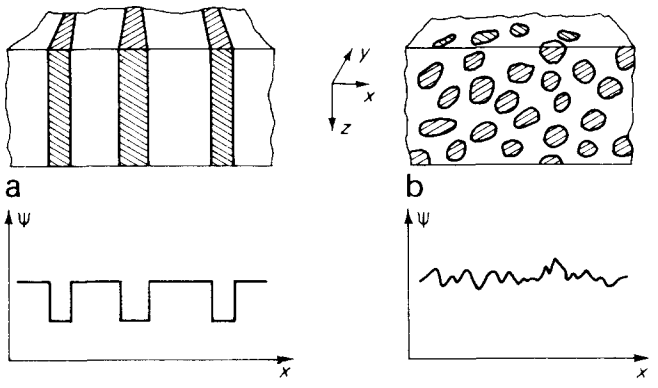

Figure 2 Cross section of two possible domain geometries for a two phase polymer film, and their resultant projected phase variations

projected potential will exhibit only random fluctuations very similar to what is expected from a pure noise object. *Figure 2a*, on the contrary, shows a geometry which yields a maximum projected phase variation. It is clear that only geometries approaching the latter type can be unambiguously analyzed, a situation more likely to occur if very thin specimen films can be prepared. The following considerations assume such an ideal model. Deviations from the model will be discussed for practical examples.

Homopolymers

The two phases are the amorphous and crystalline phases. A typical case, already well documented in the recent literature[22], is that of a polyethylene film consisting of stacks of crystalline lamellae viewed edge-on. The geometry of such a film resembles that in *Figure 2a* where the smaller domains correspond to the amorphous interlamellar zones. For this case, the relative phase change between domains is simply:

$$\Delta\psi(r) = \frac{\pi}{\lambda V_0} \frac{69}{M} \sum_i f_i \, \Delta\rho t \qquad (10)$$

The value of $\Delta\psi(r)$ may be changed by varying λV_0 (an increase of 50% from 40 kV over 100 kV) and in maximizing the film thickness, provided the same simple projected geometry is preserved. The value of $\Delta\psi(r)$ must however, remain small compared to unity (weak phase object approximation). Depending on the specific value of $\Delta\rho$, the difference in density between amorphous and crystalline phases, different optimal thickness will be obtained for each homopolymer. Density data of polymers are available from reference 23, atomic scattering factors from reference 21 or 24. If we limit $\Delta\psi(r)$ to 0.5 radians, it can for example, be calculated, that a maximum thickness of about 700 Å is possible for polyethylene and of about 1000 Å for isotactic polypropylene (100 kV). Such values are in the range of what is generally obtained experimentally, though no very precise data exists in the literature. A significantly higher nominal film thickness will result in adding an undesirable strong background from inelastic scattering and amplitude effects to the pure phase structure.

Block copolymers

Assuming two polymer sequences, (1) and (2), completely phase separated, the mean inner potential difference between the corresponding domains is, according to equation (9):

$$\Delta\bar{\varphi} = 69\left\{\frac{\rho_1}{M_1}\sum_i f_i^{(1)} - \frac{\rho_2}{M_2}\sum_j f_j^{(2)}\right\} \qquad (11)$$

As an illustration, consider a typical segmented polyurethane system consisting of hard segment (*HS*) of 4,4'-diphenylmethane diisocyanate (MDI) and 1,4 butene diol (BEDO) with soft segment (*SS*) of MDI and polypropylene oxide diol (PPO). From equation (11) we obtain $\bar{\varphi}_{HS} = 8.95$ V and $\bar{\varphi}_{ss} = 7.30$ V. If we assume the same ideal geometry as before, the phase difference of 0.5 radians between adjacent domains is obtained for a film thickness of about only 400 A (at 100 kV). As a counter example, consider the much studied polystyrene-polybutadiene system. The calculated mean inner potentials here are 7.90 and 7.82 V, respectively, leading to a completely negligible projected potential difference for usual film thickness. The possibility of phase contrast imaging of any size domains is completely ruled out in this case[25].

Other considerations

It should be mentioned that in electron microscope studies of polymers, one is always concerned with the effect of radiation damage on the observed morphology. For phase contrast imaging, possible radiation induced changes in the mean inner potential of the specimen and specimen thickness must be taken into account. If the sample consists of domains of two components and one component undergoes greater mass loss than the other, mass thickness (scattering) contrast as well as phase contrast effects may be induced by preferential electron beam etching. Changes in the mean inner potential of each type of domain may also occur due to sample mass loss and density changes. Such electron beam induced effects will lead to changes in the actual values of the inner potential and specimen thickness for each type of domain.

Also, because phase contrast is a consequence of the high coherence of the electron beam, the best contrast will be observed for the smallest beam divergence compatible with working conditions.

EXPERIMENTAL

Instrumentation

A JEOL CX 100 electron microscope was used throughout this work, at the operating voltage of 100 kV. The spherical aberration coefficient of the objective lens is 6.7 mm. An 85 μm diameter objective aperture was employed which corresponds to a 0.22 $Å^{-1}$ cut off in reciprocal space. All micrographs were recorded on Kodak SO163 film at exposure times of 2 to 4 seconds. Optical diffractograms were obtained with a Polaron instrument.

Calibration of the microscope objective lens focus increments was assumed correct. The approximate absolute value of defocus was also checked by comparison of systematically over and under focused images, with the aid of optical diffractograms.

Specimen preparation

Polymer specimens were prepared from polypropylene (Hercules Profax 6523), polyurethane

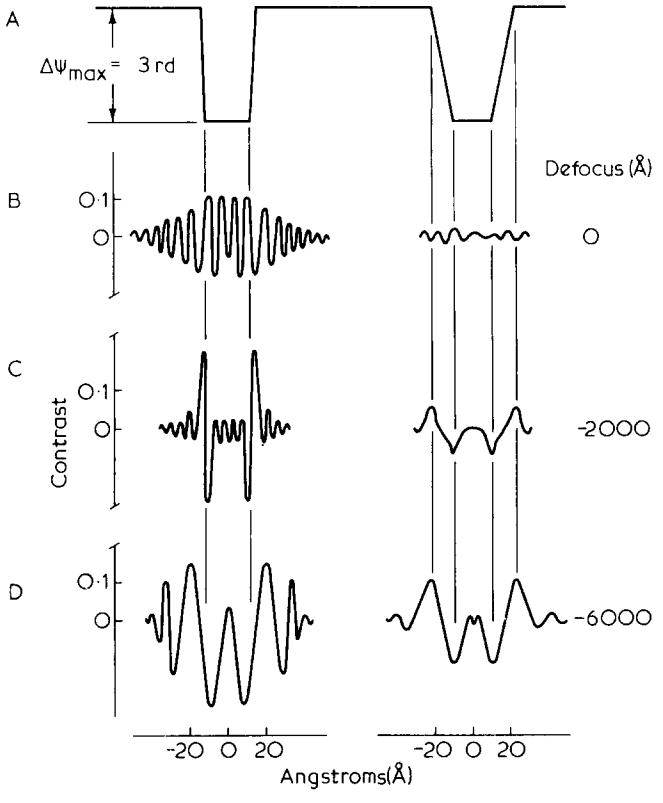

Figure 3 Effect of interface profile (A) on the image contrast of a pure phase object at small values of defocus (B–D)

PPO/MDI/BEDO*, and atactic polystyrene (Pressure Chemical Co, $M_w \sim 600\,000$ and $M_w/M_n \sim 1.1$). All films were prepared from solution casting (1% concentration). The aPS and iPP were dissolved in toluene and xylene, respectively, then cast on glycerol at 130°C. The films were picked up after a few minutes at that temperature and transferred to cool distilled water from which they were directly mounted on electron microscope grids. The urethane specimen was dissolved in DMF and cast on glycerol at room temperature, then similarly transferred to distilled water for washing. Film thicknesses were determined using the contamination spot method. By focusing a fine electron probe onto the sample (utilizing the JEOL 100 CX STEM optics) a contamination spot is produced on the entrance and exit surfaces of the polymer sample. The specimen is then tilted by 30° with respect to the incident beam direction and a micrograph of the two contamination spots recorded. Film thickness can be calculated (to ±100 Å) from the spot separation and tilt angle.

Computing

Basically, all calculations involve the use of the fast Fourier transform (*FFT*) algorithm, generally accessible from computer libraries. The data input corresponds to a series of values defining the phase profile of the object. A first application of the *FFT* operation gives a series of numbers, generally complex, which defines the Fourier spectrum of the phase function for predetermined values of the reciprocal space coordinate K. Each term of the series is then multiplied by the value of the transfer function for the same K value, and the inverse *FFT* applied to give the final contrast profile of the image.

* PPO is an ethylene oxide end capped polypropylene oxide macroglycol with $\bar{M}_n = 200$. MDI is 4,4'-diphenyl methane diisocyanate and BEDO is butenediol. The molar ratio was 1/6/5 PPO/MDI/BEDO.

Selection of a symmetrical phase profile makes calculation easier. The Fourier transforms are then defined by a series of real numbers and there is no need to define an inverse Fourier transform operation. Although such programming is very simple in principle, great care must be taken in the choice of the initial sampling period of the phase profile. Typically, the phase profile was sampled at intervals of 2 Å in the present calculations. This in turn gives a Fourier spectrum calculated by steps of 0.001 $Å^{-1}$ which allows a proper sampling of the sin χ function even at very high defocus. Although not presented here, two dimensional calculations following the same scheme are perfectly feasible.

Model calculations

The model object selected corresponds to an approximately periodic arrangement of two phases in a film similar to the one represented in *Figure 2a*. The domains are of 25 and 100 Å width respectively, so that the model may represent the typical succession of amorphous and crystalline zones in semicrystalline homopolymer thin films. The maximum phase change is taken to be 0.3 radians. This model gives the phase profile of *Figure 3A*. Two types of interface are represented. The first one (*Figure 3A*, left) defines a sharp boundary of only 2 Å thickness. *Figures 3B*, *3C* and *3D* show the corresponding image contrast for 0 Å, −2000 Å, and −6000 Å defocus (underfocus). With the sign conventions used here, positive contrast in *Figures 3* and *4* corresponds to bright or dark contrast in the micrographs (positives) depending on whether the small domains represent respectively crystalline or amorphous domains. In the following the smaller domains represent amorphous domains, i.e., domains of

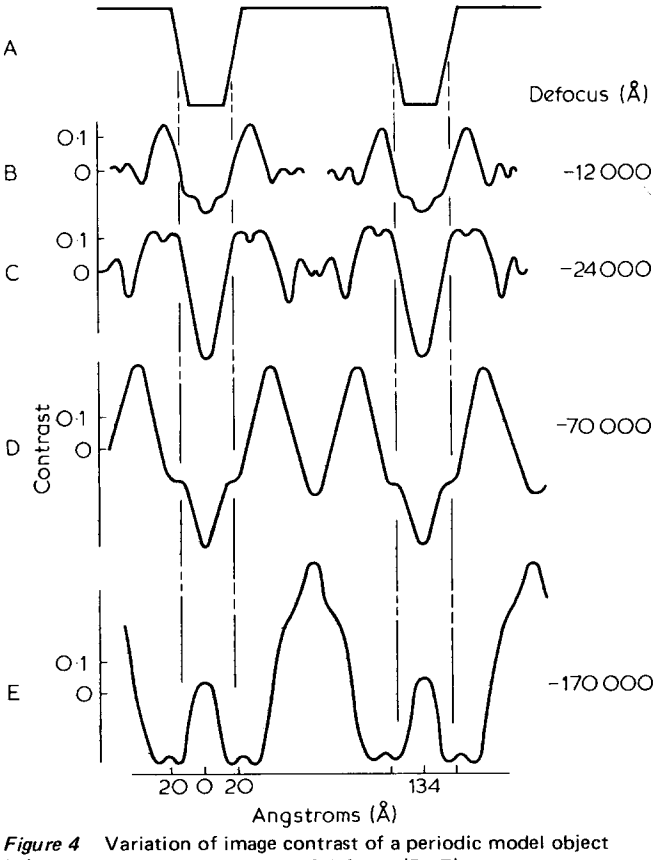

Figure 4 Variation of image contrast of a periodic model object (A) at medium and large values of defocus (B–E)

lower mean inner potential. The best values of defocus, in terms of faithful representation of the object function by the phase contrast, is that for which the sin χ curve approaches unity over the largest interval in the reciprocal space coordinate system. This optimum defocus value is specific to the C_s value of the microscope [see equation (4)], and was determined here to be close to -2000 A (see Figure 1). *Figure* 3*C* (left) illustrates how the choice of this value of defocus theoretically allows a very precise imaging of the sharp interface which is marked by a pair of narrow bright and dark fringes. The width of the fringes is, however, totally unresolvable in practical operation. At optimum focus, therefore, the domain structure is not imaged.

The nominal zero value of defocus gives some contrast because of the residual phase shift due to the nonvanishing spherical aberration term in equation (4). It consists of a packet of fringes (*Figure* 3*B*, left) also impossible to resolve practically. Going to higher underfocus (*Figure* 3*D*, left) creates a pair of larger and stronger fringes still centred about the boundary and with noticeable secondary fringes. Increasing the microscope defocus thus results in an increase of image contrast at the expense of resolution (fringe width).

Many studies, particularly small angle x-ray scattering studies, have been devoted to the determination of the interface profile in phase separated polymeric systems. However, due to the complexity of the problem, various models exist[26-29]. We consider here a model of 'linear' interface of 12 A thickness (*Figure* 3*A*, right) corresponding to data in reference 27. Other profile shapes have been considered in a previous publication[30]. Smoothing the interface profile results, essentially, in a reduction of the intensity and number of the fringes, as shown in *Figures* 3*B*, *C* and *D* (right). Again, optimum defocus gives the best definition of the interface, but at a very low contrast. For -6000 A defocus, the contrast improves but is more difficult to detect than for the step interface model.

Figure 4 presents a series of contrast profiles of the same object (ramp interface) obtained at increasing values of underfocus. A dramatic increase in contrast is observed at values of defocus between 12000 and -24000 A when fringes marking the opposite boundaries of the small domain begin to overlap. The maximum contrast reaches 35% in *Figure* 4*C*. The contrast between the larger fringes outside the domain and the background is, however, only about 10% so that these fringes will not appear in the image. The image will most likely consist of rows of domains of about 20 A width, within a background which will represent the larger domains. The defocused image is then a fairly good representation of the actual structure. The sin χ function is antisymmetrical with respect to ΔZ (defocus) for high values of ΔZ, so that the image would approximately reverse contrast when changing the sign of defocus. The contrast can be enhanced further at even higher defocus values. This is shown in *Figures* 4*D* and 4*E* which correspond to -70000 A and -170000 A defocus, respectively. Contrast goes up to 50% with simultaneous increase in the fringe width. The correspondence between the actual structure and the resulting image is, however, lost. In *Figure* 4*D*, a dark fringe appears in the middle of the large domain and contrast reverses between *Figure* 4*D* and 4*E*. This makes interpretation of the profiles unreliable. Although the higher amounts of defocus lead to more contrasted calculated profiles, there appears to be an optimum defocus for phase contrast imaging of about ± 20000 A for the present model. This value of objective lens defocus is of course dependent on the size of the domains taken in the model. A model composed or larger (smaller) domains, i.e. corresponding to lower (higher) spatial frequencies, would give the types of contrast profiles as shown in *Figures* 4*B* to 4*E* for higher (lower) values of defocus.

To make interpretation of the calculated profiles easier, the noise background, although it may play a decisive role, has not been considered in the selected phase profiles. This important point will be discussed when considering experimental images.

DISCUSSION OF EXPERIMENTAL IMAGES

Amorphous and crystalline contrast in homopolymer films

As discussed above, a high phase contrast image is expected from polyethylene films with proper domain orientations. Such a case has been described initially by Peterman and Gleiter[22]. Precise comparison with the present calculation is difficult as some of their parameters are not clearly defined. The average size of the crystalline domains (250 A) is also larger than that selected here. Nevertheless, the width of the amorphous domains, as measured from the in-focus image in their paper, is only slightly higher than that in our model. A qualitative comparison is thus possible if we limit it to defocus values not greater than about 30000 A where fringes within the large domains in *Figure* 4 begin to overlap (the fringes would not yet overlap for 250 A crystalline domains). Peterman and Gleiter report defocus values of the order of 10000 A or more (imprecise) in order to obtain good contrast. These values are in reasonable agreement with those determined above (see *Figure* 4*B* and 4*C*). It must also be noted that the in-focus image as shown in their paper does exhibit enough contrast (mass-thickness contrast) to sufficiently characterize the structure.

In order to evaluate the capabilities of the phase contrast technique on a less favourable case, we have studied the structure of isotactic polypropylene films. This polymer, all other conditions being equal, gives 30% less phase difference between amorphous and crystalline domains, as calculated above. The films were prepared by solution casting at high temperature at conditions ecpected to give a suitable film geometry[31]. No further annealing treatment to enhance the crystallinity and phase separation was performed. The films were rather unstable under the electron beam and crystallinity was readily destroyed during image recording. As a consequence, the actual density difference between the previously crystalline domain and the amorphous ones was certainly lowered. Less phase contrast than theoretically possible is then to be expected.

Figures 5*a* to 5*d* are an under-focus series, taken in the order shown, of an area of such a film. The electron micrograph shown in *Figure* 5*a* is close to focus - no contrast other than that arising from large scale mass-thickness fluctuations is apparent. For medium values of underfocus, i.e., -20000 A and -37000 A (*Figures* 5*b*) and 5*c*) careful examination of the images reveals narrow ($\sim$80 A) elongated dark lines grouped in parallel, more visible in *Figure* 5*c*. At higher defocus, i.e., -71000 A (*Figure* 5*d*), the contrast is further enhanced. The dark lamellar domains are 150 to 300 A apart. Such features indicate the presence of crystalline domains approxi-

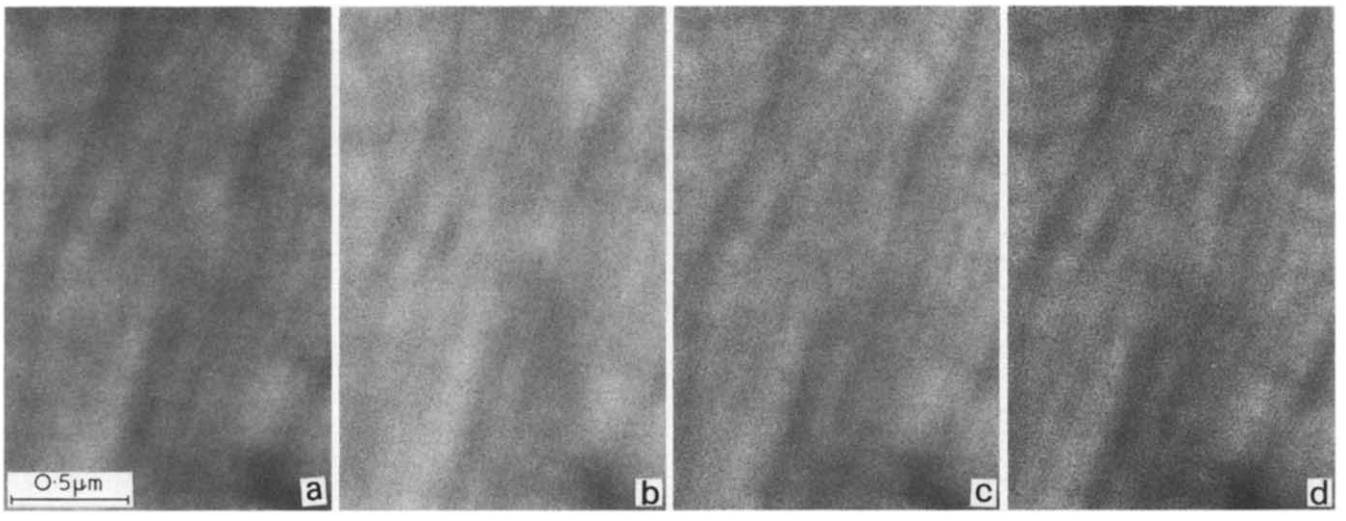

Figure 5 Underfocus series (in steps of 17 000 Å) of part of a polypropylene film showing the progressive appearance of the lamellar structure. Defocus in (a) is ~−3000 Å

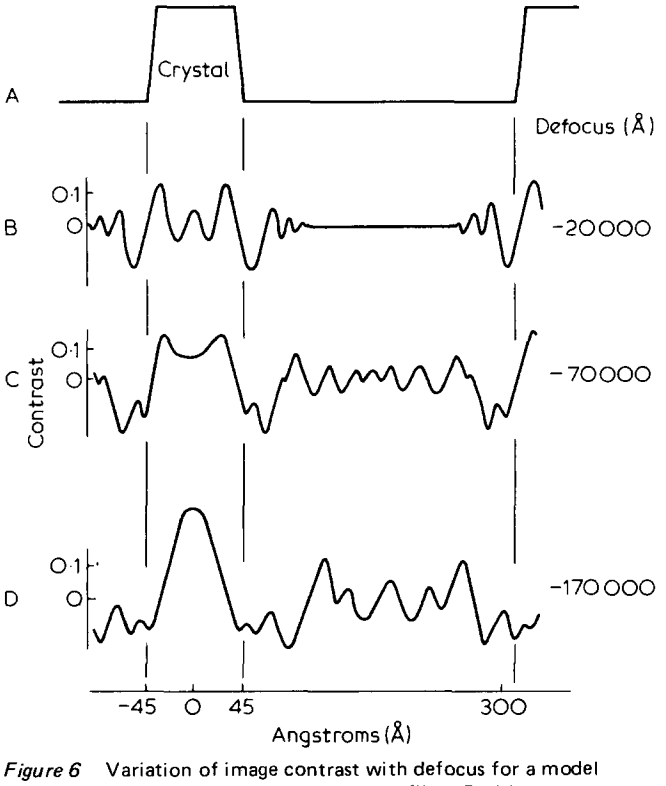

Figure 6 Variation of image contrast with defocus for a model object corresponding to the polypropylene film. Positive contrast corresponds to dark regions in micrograph print

mately 80 Å thick separated by wider less dense domains.

Understanding of the contrast enhancement mechanism cannot be derived from the model presented in *Figure* 4. A model characterized by amorphous domains larger than the crystalline ones is needed. Such a model is presented in *Figure* 6*A* where the amorphous and crystalline domains are respectively 300 and 80 Å thick with the same interface profile as in *Figure* 4*A*. The calculated contrast profiles in *Figures* 6*B* and 6*C* account well for the variation of contrast observed in *Figure* 5. Because of the larger domain sizes the optimum value of defocus for phase contrast enhancement is now close to −70 000 Å instead of about −20 000 Å for the model selected in *Figure* 4. Validity of the assumed specimen geometry is

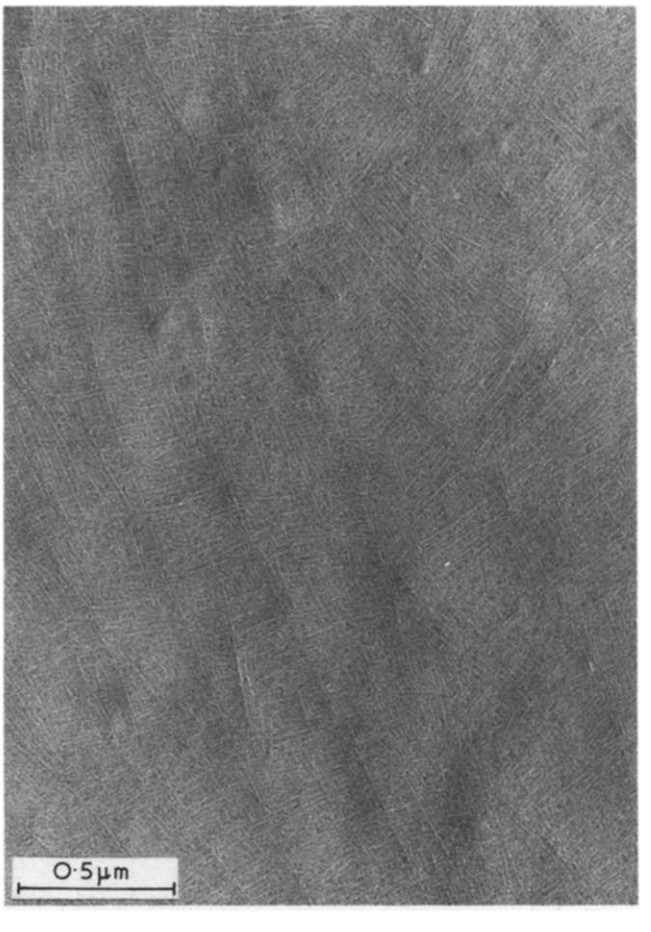

Figure 7 Cross-hatched structure of the polypropylene film as revealed by metal decoration (Au/Pd)

ascertained by *Figure* 7 which shows a gold/palladium decorated area of the same film, where the dark regions are now amorphous zones because of mass thickness contrast due to their selective metal decoration. The characteristic cross-hatched structure of polypropylene[32] is revealed. The crystalline lamellae are 80 to 100 Å thick and 200 Å or more apart. A low contrast structure is also noticeable. It consists of closely packed lamellae with interlamellar amorphous zones only 20 to 40 Å thick.

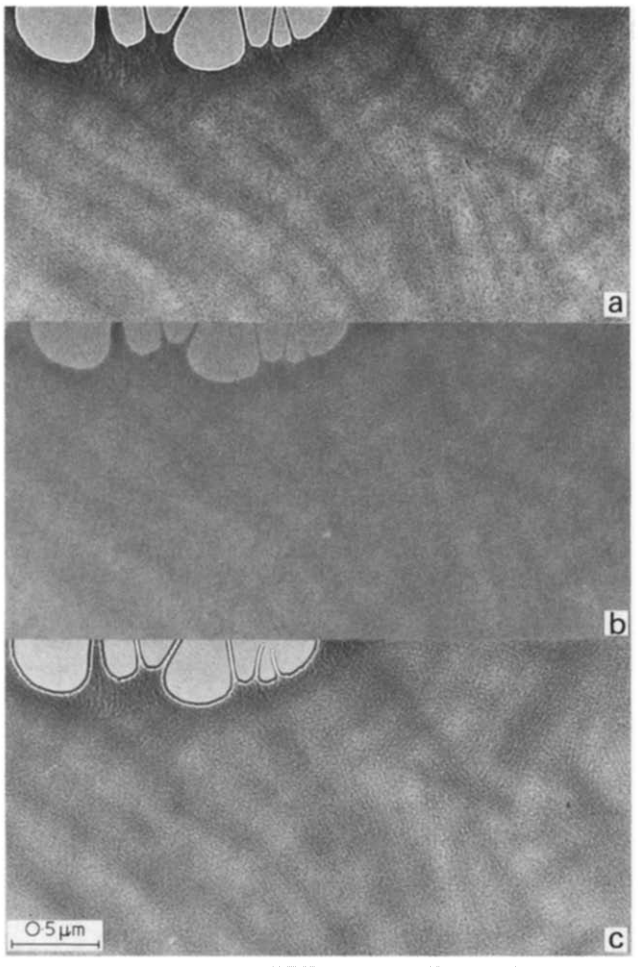

Figure 8 Through focus series of a polypropylene film. Respective values of defocus are a, −170 000 Å; b, ~−3000 Å; and c, +170 000 Å; note the reversal of contrast between (a) and (c)

This substructure was not revealed by the defocus technique because the contrast enhancement is too weak.

There are several reasons for the faintness of the defocus contrast here. First there is the 30% difference in expected contrast as compared to PE and loss of crystallinity from beam damage*. A second reason may be the result of too large a film thickness (estimated to be about 1000 Å). Second order effects will then not be negligible and a higher background level would be obtained. Finally, geometrical factors may well be the most important ones. Poor orientation of the lamellae with respect to the electron beam (the films have not been submitted to an orientation treatment) would make the interface phase profile much smoother than represented in *Figure* 4*A*, but the amorphous zones would still be accessible to the evaporated metal atoms.

Figures 8*a*, 8*b* and 8*c* present images from the same PP film at −170 000 Å defocus, at about focus and at +170 000 Å defocus respectively. Near focus, the phase contrast is absent. At low to medium defocus, images (not shown here) show the same limited contrast as illustrated in *Figures* 5*c* and 5*d*. In *Figures* 8*a* and 8*c*, on the contrary, the cross-hatched structure is very well suggested by series of parallel dark and bright bands of about 100 to 150 Å width and elongated over 1 μm in some cases. This dramatic increase in contrast was predicted by the calculations (*Figure* 6*D*). The change in the apparent size of the bands may also be an important factor in the subjective perception of contrast as the human eye is sensitive to certain particular frequencies[33] precisely in the range of these here present. A nearly perfect reversal of contrast between the two figures is noticed, indicating that this area of the film is a good approximation of a weak phase object, although mass thickness contrast is indeed present as a background fluctuation. The width of each type of domain is now comparable, about 100 and 150 A, so that distinction between the overfocused and underfocused image would be very difficult without the help of the holes. According to *Figure* 6*D* the dark bands in the underfocused image should remain centred on a crystalline zone, but identification of a particular domain from a single image may be hazardous without the help of a complete through focus series.

The optical diffractogram corresponding to these defocused images is shown in *Figure* 9. It appears composed of two different contributions. The circular pattern arises from the modulation of the noise structure by the transfer function of the electron microscope. Four spots can also be distinguished superposed onto the inner ring of this diagram (the schematic helps recognition). They define the diffraction pattern of the cross-hatched structure.

Present observations indicate that the theoretical predictions of contrast from simple film geometries are well verifed. By using very large defocus values, weak phase structures in the size range usually encountered in semicrystalline polymer films can be enhanced enough to allow a rough characterization of the morphology. The resolution of the images, however, does not compare with that obtained from more usual techniques like heavy atom decoration.

Complex structures

The question now under consideration is whether it is safe to extend the results obtained on simple structures to more complex systems, as recently stated[15]. To clarify this point, we have studied the defocus imaging of films of a segmented polyurethane based on the PPO/MDI/BEDO system, which has been shown in the calculations above to give sufficient phase contrast for model structures. Direct electron microscope observations in similar systems of a domain structure associated with the segregation of the hard and soft segments have repeatedly been published in

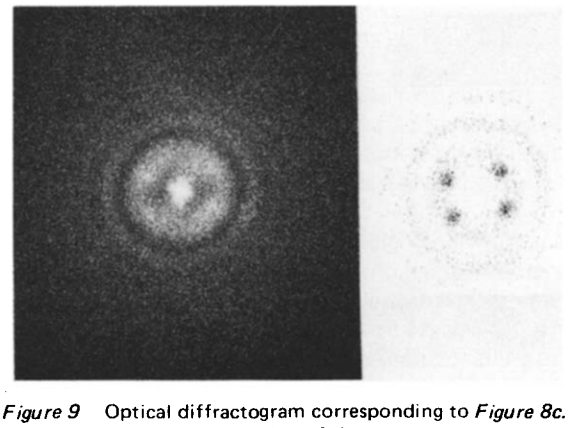

Figure 9 Optical diffractogram corresponding to *Figure 8c*. The schematic indicates the position of the spot pattern corresponding to the cross-hatched structure

* After the initial loss of crystallinity, further possible beam damaging effects appear to interfere only very slightly with phase contrast effects. This was verified by changing the recording order of the defocus series.

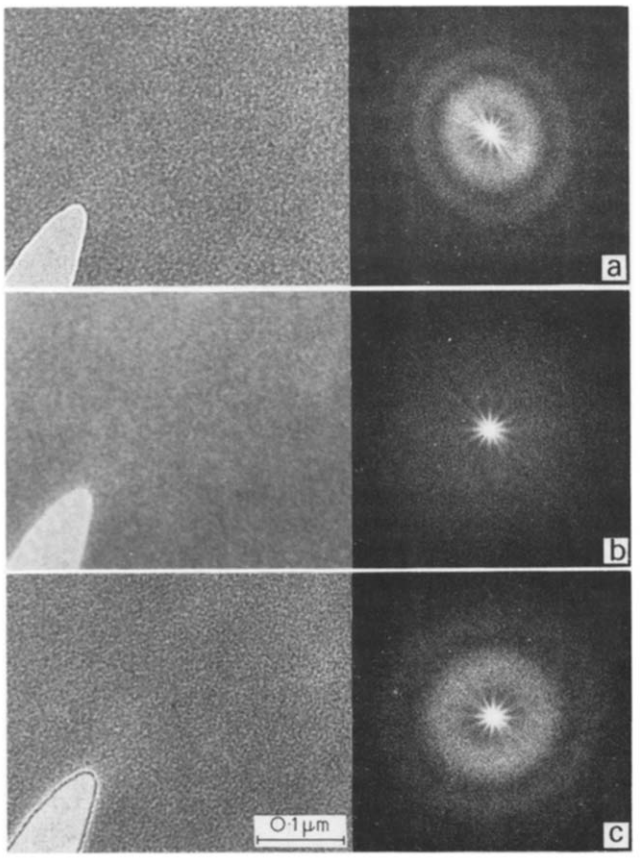

Figure 10 Through-focus series and corresponding optical diffractogram of part of a polyurethane film (MDI/PPO/BEDO). Defocus values are a, −20 000 Å; b, −3000 Å; and c, +14 000 Å

the last years[12-15]. Part of the film is shown in Figure 10 which presents a through focus series for defocus values of about −20 000, −30 000 and +14 000 Å, respectively. In order to search for a possible domain structure in the 50 Å to 200 Å range, film thickness must also be within this range. Estimation of the thickness of the polyurethane film indicated that this condition was fulfilled. The size of the structure observed is a direct function of the absolute value of defocus, which is a feature typical of the noise structure[34]. The optical diffractograms inserted in the figures confirm this observation (the minima observed are determined by the zeros of $\sin^2 \chi$). The larger 'domain' sizes in *figure 10a* are about 40 Å as compared to 30 Å for those in *Figure* 10*c*, which correspond to higher frequencies in the diffraction plane. Closer to optimum focus (*Figure* 10*B*) no such contrast is seen in either the image or the diffractogram. Here the transfer function is monotonously varying for most of the frequency range corresponding to the resolution of the image (15 Å).

As a defocused image will always consist of the superposition of the enhanced domain structure if there is one, and the filtered noise structure, it is interesting to compare images of different specimens recorded under the same optical conditions. Images of the polyurethane film, a carbon film and a polystyrene film, respectively, are presented in *Figures* 11*a*–11*c*. They have been taken at 20 000 magnification to limit radiation damage. This magnification allows a final resolution of about 15 Å, a value sufficient for the present investigation. The optical diffractogram inserts to the images show the similarity of the defocus conditions in each experiment, i.e., about 20 000 Å (absolute value). A few minor differences can be noted between the figures. The evaporated carbon film and the polyurethane film give the most contrasted structures and this is attested by the greater number of rings visible in the diffraction patterns. The images of the carbon film, the polyurethane film and the PS film were taken during the same session, i.e., with the same slight astigmatism.

It is also interesting to note in *Figure* 11*c* how an increase of the film thickness weakens the phase structure. In a previous paper, thinner films of the same polymer were found to behave as pure phase objects[11]. Except for these limited differences, the structures observed in all images appear fundamentally the same; the images are dominated by the spatially filtered noise structure. The variation of the size of the noise structure with defocus for PP films is also illustrated by the series of micrographs in *Figure* 5. For the films considered in *Figure* 10, larger amount of defocus do not reveal any additional structure.

How does this structure common to all the films (carbon, PS and polyurethane) compare with previous observations of polyurethane morphology? Among these studies, two deliberately used the defocus technique[14,15] at optical conditions which were probably close to those used here. In other papers[12,13] defocusing was apparently not intentional. Nevertheless, all images closely resemble those shown in *Figure* 9 and are then perfectly explained by the same causes. Any discrepancy between the sizes of the 'domain' structure from one paper to the other must be attributed to different defocusing conditions. Specimen drift, objective lens astigmatism, or aperture misalignment would result in apparent elongated domains.

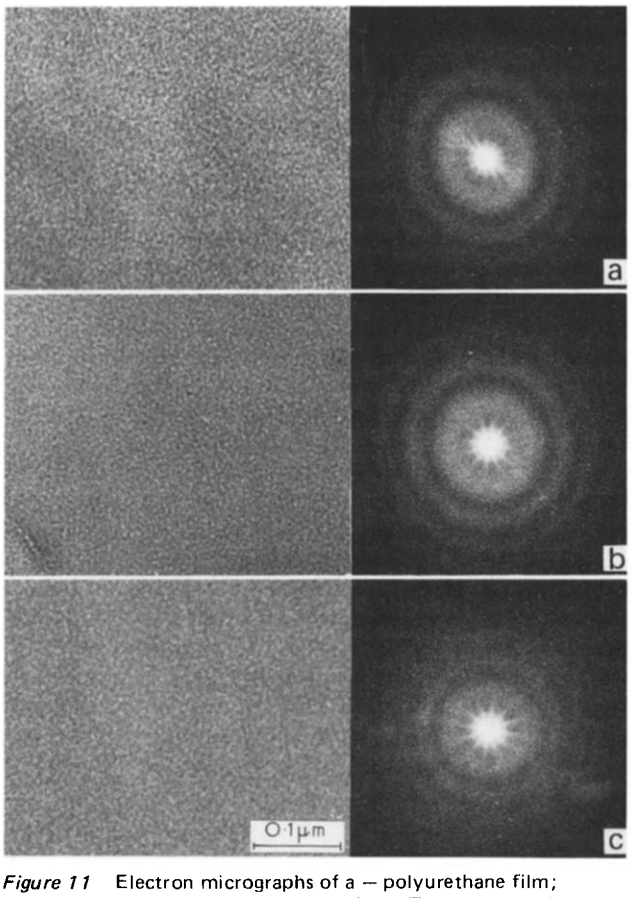

Figure 11 Electron micrographs of a — polyurethane film; b — carbon film; and c — polystyrene film. The corresponding optical diffractograms attest to the similarity of the defocus conditions in each case

As a consequence, no reliable information about the actual structure of polyurethane and other complex systems can be derived from such images. Because the apparent domain size depends on both the size of the potential fluctuations and upon the transfer function, differences in the high resolution noise structure of a wide range of amorphous materials is still under study to determine the exact nature of the amorphous 'order'[35]. Such studies are outside the goals of the present work.

CONCLUSIONS

Efforts have been made to clarify the common misconception of casually interpreting dark regions in medium resolution bright field electron micrographs of phase separated polymers directly as higher density domain structures in the polymer film. The main result of our investigation into phase contrast imaging of polymer microstructures is to clearly identify the images as essentially determined by the microscope transfer function[11]. In the case of simple phase separated structures, provided the interpretation is based on a complete through focus series, this technique does provide a faithful image of enhanced contrast. It must be noted however, that the corresponding structures have for a long time been identified by other simple microscopy techniques. More interesting is the case of complex polymer systems for which the supposed domain structure has been deduced partly from defocused electron micrographs. To decide whether the observed image features are related to real domains in the object or are simply due to the microscope spatial frequency filtering of a homogeneous random array of scatters is quite difficult, since images of completely different object models are qualitatively indistinguishable. Faithful image reconstruction of the object structure by phase contrast imaging only occurs when the transfer function is the same and near unity for all the important object spatial frequencies. For irregular domain structures, it is not possible to reconstruct reliably the projected potential variations of the object. Even if the image system were perfect, it would be difficult to determine the true object structure from the recorded image, unless the domain size is of the order of the film thickness, since the image is a two dimensional projection of the complex three dimensional domain morphology of the specimen.

High resolution bright field electron micrographs of unstained polymer films previously published contain no reliable information on the actual micromorphology. The published micrographs are dominated by spatially filtered noise. For this reason, it is essential to employ scattering contrast to image small scale domain structures. For polymer systems containing ordered domains this would indicate dark field imaging and for microphase separated multicomponent polymer systems, heavy atom staining. The PPO/MDI/BEDO urethane system has been successfully investigated with the latter technique[36].

ACKNOWLEDGEMENTS

The authors are indebted to Dr. T. Takahashi for providing the micrograph of Figure 6.

Acknowledgement is made to the Materials Research Laboratory of the University of Massachusetts and to the National Science Foundation, Grant DMR 77 24955, Polymers Programme, for financial support. One of us (EJR) thanks the CNRS for permitting his stay at the University of Massachusetts.

REFERENCES

1 Heidenreich, R. D. 'Fundamentals of Transmission Electron Microscopy' Interscience, New York, 1964, 140
2 Erickson, H. P. and Klug, A. *Ber. Bunsen. Gesell.* 1970, **74**, 1129
3 Yeh, G. S. Y. and Geil, P. H. *J. Macromol. Sci. (Phys.)* 1967, **B1**, 235
4 Yeh, G. S. Y. *Crit. Rev., Macromol. Chem.* 1972, **1**, 173
5 Klement, J. J. and Geil, P. H. *J. Macromol. Sci. (Phys.)* 1972, **B6**, 31
6 Carr, S. H., Geil, P. H. and Baer, E. *J. Macromol. Sci. (Phys.)* 1968, **B2**, 13
7 Frank, W., Goddar, H. and Stuart, H. A. *J. Polym. Sci.* 1967, **C5**, 711
8 Siegmann, A. and Geil, P. H. *J. Macromol. Sci. (Phys.)* 1970, **B9**, 239
9 Luch, P. and Yeh, G. S. Y. *J. Appl. Phys.* 1972, **43**, 4326
10 Flory, P. J. *J. Macromol. Sci. (Phys.)* 1976, **B12**, 1
11 Thomas, E. L. and Roche, E. J. *Polymer* 1979, **20**, 1413
12 Wilkes, G. L., Samuels, S. L. and Crystal, R. *J. Macromol. Sci. (Phys.)* 1974, **B10**, 203
13 Koutsky, J. A., Hein, N. V. and Cooper, S. L. *J. Polym. Sci., Polym. Letters* 1970, **8**, 353
14 Chang, A. L. and Thomas, E. L. 'Adv. in Chem. #176, Multiphased Polymers' (Ed. S. L. Cooper and G. M. Estes) 1979, 31
15 Miles, M. J. and Petermann, J. *J. Macromol. Sci. (Phys.)* 1979, **B16**, 243
16 Johnson, D. J. and Crawford, D. *J. Microsc.* 1973, **98**, 313
17 Agar, A. W. and Alderson, H. 'Principles and Practice of Electron Microscope Operation', in Practical Methods in Electron Microscopy (Ed. A. M. Glauert) Elsevier New York, 1974, 277
18 Hanszen, K. 'Advances in Optical and Electron Microscopy, 4', (Ed. R. Barer and V. E. Cosslett), Academic, London, 1971
19 Erickson, H. P. 'Advances in Optical and Electron Microscopy, 5', (Ed. R. Barer and V. E. Cosslett), Academic, London, 1973
20 Cowley, J. M. 'Diffraction Physics', North-Holland, Amsterdam, 1975
21 Vainshtein, B. K. 'Structure Analysis by Electron Diffraction', Pergamon Press, Oxford, 1964
22 Petermann, J. and Gleiter, H. *Phil. Mag.* 1975, **31**, 929
23 Wunderlich, B. 'Macromolecular Physics', Academic Press, Vol. 1, 1973, 388 9
24 Doyle, P. S. and Turner, P. S. *Acta Cryst.* 1968, **A24**, 390
25 Hedren, A. and Thomas, E. L. unpublished results
26 Ruland, W. *J. Appl. Cryst.* 1971, **4**, 170
27 Vonk, C. G. *J. Appl. Cryst.* 1973, **6**, 81
28 Bonart, R. and Müller, E. H. *J. Macromol. Sci., Phys.* 1974, **B10**, 177
29 Hashimoto, T. and Kawai, H. *Macromol.* 1977, **10**, 377
30 Christner, G. L. and Thomas, E. L. *J. Appl. Phys.* 1977, **48**, 4063
31 Thomas, E. L. and Takahashi, T. to be published
32 Padden, F. J. Jr. and Keith, H. D. *J. Appl. Physics* 1966, **37**, 4013
33 Ratliff, F. *Sci., Am.* 1972, **226**, 90
34 Thon, F. *Z. Naturforsch.* 1966, **21a**, 476
35 Gaskell, P. H. and Mistry, A. B. *Phil. Mag.* 1979, **39A**, 245
36 Fridman, I. D. and Thomas, E. L. *Polymer*, 1980, **21**, 388